Materials Science & Engineering A 872 (2023) 144982

Contents lists available at ScienceDirect

Materials Science & Engineering A

journal homepage: www.elsevier.com/locate/msea

Anomalous fatigue crack propagation behavior in near-threshold region of L-PBF prepared austenitic stainless steel

Michal Jambor [a,*], Tomáš Vojtek [a], Pavel Pokorný [a], Daniel Koutný [b], Luboš Náhlík [a], Pavel Hutař [a], Miroslav Šmíd [a]

[a] *Institute of Physics of Materials, Czech Academy of Sciences, Žižkova 513/22, 616 00, Brno, Czech Republic*
[b] *Faculty of Mechanical Engineering, Institute of Machine and Industrial Design, Brno University of Technology, Technická 2896/2, 616 69, Brno, Czech Republic*

ARTICLE INFO

Keywords:
Fatigue crack propagation
Laser powder bed fusion
Austenitic stainless steel
Crack closure
TRIP

ABSTRACT

Laser powder bed fusion (L-PBF) process produces a specific non-equilibrium microstructure with properties significantly different from those of conventionally processed materials. In the present study, the near-threshold fatigue crack propagation in austenitic stainless steel 304L processed by L-PBF was investigated. Three series of specimens with different orientation of initial notch with respect to build direction were manufactured in order to evaluate the effect of specimen orientation on the near-threshold fatigue crack propagation behavior. The results showed absence of the orientation dependence of the fatigue crack propagation behavior. In addition, abnormally low threshold stress intensity factor values were recorded, which were attributed to the absence of crack closure even at low load ratio ($R = 0.1$). In order to explain observed behavior, the specimens of selected orientation were heat treated to relieve build-in residual stresses (HT1) and to create recrystallized microstructure (HT2) comparable to conventionally processed (wrought) stainless steels. It was found that the characteristic microstructure produced by L-PBF is the main reason for the absence of crack closure and the low threshold values at low load ratios. As-built microstructure containing sub-micron dislocation cell-substructure is prone to cyclic instability. In the crack tip region, cyclic plasticity results in strain-induced phase transformation and continuous thin martensitic layer is formed in the crack vicinity. The induced martensite phase is softer compared to the austenite matrix strengthened by cell-substructure. Together with cyclic instability of the matrix, the macroscopic cyclic softening occurs as the result within the crack tip region. Under such conditions, the formation of the plasticity-induced and roughness-induced crack closure is significantly reduced and macroscopic resistance to the fatigue crack propagation is low.

1. Introduction

Since introduced, additive manufacturing (AM) became an important material processing method, offering several significant advantages over traditional processing techniques. The most important advantage over conventional processing routes is high design freedom and low waste due to absent machining process [1,2]. Besides that, AM methods often produce materials with specific microstructures, which can be beneficial in terms of the resulting properties [3–5]. Laser powder bed fusion (L-PBF) is one of the most widespread AM methods, in which powder bed is selectively melted by scanning laser beam in layer-wise manner [6]. During L-PBF process, extremely fast solidification occurs, with the cooling rates reaching values of 10^6 K s^{-1} [7,8]. This results in formation of specific solidification microstructures with an interesting combination of mechanical properties. Microstructure characterization of austenitic stainless steels prepared by L-PBF was the subject of numerous studies in recent years. It was found that the rapid solidification results in a formation of the characteristic cell-substructure, with a very high dislocation density within the cell walls [3–5]. This configuration offers a significant strength enhancement due to the Hall-Petch strengthening [9,10].

With rapid development of the AM in recent years, there was a lot of attention attributed to the evaluation of the properties of austenitic stainless steels processed by L-PBF. Mechanical properties of 316L grade steel in as-built and heat-treated conditions were studied by Salman et al. [11], Chen et al. [12], and Yin et al. [13]. Fatigue properties and the effect of heat treatment were addressed in works of Blinn et al. [14], Zhang et al. [5] and Elangeswaran et al. [15]. Shin et al. [16] studied

* Corresponding author.
E-mail address: jambor@ipm.cz (M. Jambor).

https://doi.org/10.1016/j.msea.2023.144982
Received 31 January 2023; Received in revised form 15 March 2023; Accepted 28 March 2023
Available online 31 March 2023

wear properties, while the high-temperature tensile properties were examined by Dryepondt et al. [17]. Finally, corrosion behavior was studied by Kong et al. [18] and Chao et al. [19]. Despite the focus of many researchers on the topic of L-PBF-processed austenitic steels, the number of published articles dealing with fatigue crack propagation is limited, and several aspects of this phenomenon remain unclear. Considering the growth of fatigue cracks to be one of the most frequent failure modes in engineering applications [20], a thorough analysis of various aspects of fatigue crack propagation behavior in stainless steels produced by L-PBF is still needed. Riemer et al. [21] examined the fatigue crack propagation behavior of L-PBF processed 316L steel. They found differences in the crack growth properties for differently oriented samples with respect to the built direction (BD). Recorded variations were attributed to different behavior when a crack propagates along/-perpendicular to the long axis of columnar grains. The role of the BD on the crack propagation behavior of L-PBF processed austenitic steels was also reported by Suryawanshi et al. [22]. Additionally, Zhu et al. [23] reported higher resistance of L-PBF 304L grade steel to the fatigue crack propagation under hydrogen embrittlement compared with the conventional counterpart, which was attributed to the suppressed twin and α′ martensite formation frequently observed in L-PBF processed steels. Riemer et al. [24] also showed a strong relation between L-PBF processing parameters and the fatigue crack propagation resistance in as-built (AB) condition. On the other hand, Kumar et al. [25] revealed that the fatigue crack propagation of L-PBF 304L steel was insensitive to the BD. This study also reported significant influence of the stress-induced martensitic transformation in the crack tip plastic zone on the crack opening displacement (COD) and, thus, to the crack propagation rate. However, in their work, more attention was paid on the behavior in the Paris region, while the behavior close to threshold stress intensity factor (SIF) was not addressed. Riemer at el [21]. reported threshold SIF (ΔK_{th}) for stress ratio $R = 0.1$ to be between 3 and 4 MPa m$^{1/2}$, depending on the sample orientation with respect to BD. This is significantly less than the values recorded by Jambor et al. [26] for wrought 304L steel (5–7 MPa m$^{1/2}$). Similarly low ΔK_{th} were reported also by Fergani et al. [27], but clear explanation for such values hasn't been presented so far. As was shown in study of Pokorný et al. [28], even a small change in the threshold value of SIF can have a significant effect on the total residual lifetime of structurally loaded parts. Therefore, the understanding and detailed description of fatigue crack propagation behavior in the near-threshold regions is of utmost importance for successful and effective application of AM parts in cyclically loaded engineering structures.

The present study focuses on fatigue crack propagation in L-PBF processed austenitic stainless steel 304L in the near-threshold region. Three types of compact tension (CT) specimens, varying in different orientation of crack propagation direction with respect to the BD, were used to clarify possible effect of specimen orientation on the fatigue crack propagation behavior. Subsequently, specimens of one orientation underwent two different heat treatments to shed a light on the effect of characteristic L-PBF microstructure on fatigue crack behavior and to clarify the recorded low threshold SIF.

2. Material and experiment description

2.1. Material and specimen preparation

Gas-atomized powder of 304L austenitic stainless steel (supplied by Sandvik Ltd.) of chemical composition shown in Fig. 1 was used as the feedstock material. Blocks with dimensions 40 × 40 × 40 mm were fabricated by L-PBF method using a SLM 280HL machine (SLM Solution Group AG) equipped by an Yb-fiber laser with maximum power of 400W and spot size diameter of 80 μm. A 100 × 100 mm build plate was kept heated at 100 °C and the machine chamber was constantly flushed by nitrogen. For the fabrication of blocks, the laser power operated at 235 W while scanning speed, hatch distance and layer thickness were set to 790 mm s^{-1}, 120 μm and 50 μm, respectively. In order to obtain random crystallographic orientation of microstructure, the laser scanning direction was rotated by 67° after every finished layer. Subsequently, CT specimens were conventionally manufactured from the blocks in three different orientations, as depicted in Fig. 1. Further details regarding of the CT specimens dimensions can be found in Ref. [26]. Tensile properties were evaluated using cylindrical specimens with gauge length of 35 mm and diameter of 6 mm, with loading axis oriented perpendicular to BD. Tests were performed in accordance with EN ISO 6892-1, using a tensile testing machine Zwick Z50 at constant strain rate of 1 mm min^{-1}.

Powder chemical composition in wt.%

C	Cr	Ni	Mn	S	P	Si	Fe
0.023	18.12	8.18	1.79	0.003	0.04	0.17	Bal

Basic mechanical properties:

UTS 780 MPa
YS 592 MPa
El. 49%
E 195 GPa

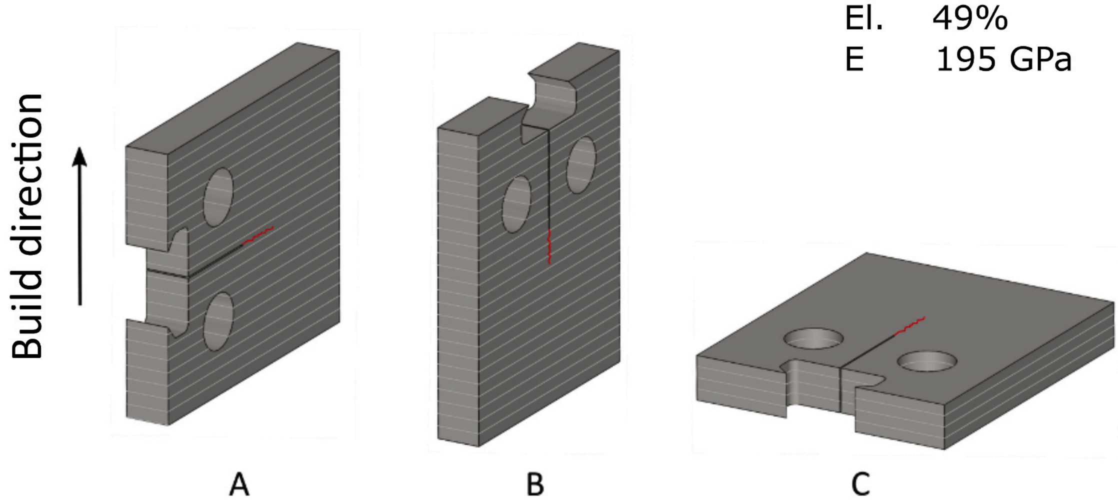

Fig. 1. Chemical composition of the used 304L powder and basic mechanical properties in as-built condition. Three series of CT specimens with different orientation of crack propagation direction with respect to the build direction were manufactured.

Yield strength of 592 MPa, ultimate tensile strength of 780 MPa and total elongation at fracture of 49 % was obtained.

In order to explain the recorded fatigue crack propagation behavior and to assess the influence of L-PBF microstructure, the specimens of A orientation (according to Fig. 1) were used for further investigation. Three distinct microstructural states of L-PBF processed 304L steel were examined: as-built (AB) and two heat-treated conditions. The heat treatment 1 (HT1) consisted of annealing at 650 °C for 4 h, to relieve residual stresses, while the initial microstructure remains intact. The similar parameters of stress-relieving heat treatment were used in Refs. [21,27]. The second heat treatment (HT2), annealing at 1100 °C for 4 h, represents a nearly fully recrystallized microstructure, with a polyhedral grain structure, similar to the microstructure of conventional wrought material. The heat treatments were carried out in a resistance furnace in argon protective atmosphere and specimens were subsequently air cooled. The change in the mechanical properties after applied heat treatment was addressed by hardness measurement. Tests were carried out according to standard EN ISO 6507. For each tested state, a set of 10 indentations was performed using Zwick ZHμ Vickers hardness tester applying load of 9.8 N and subsequently the average hardness values were calculated.

2.2. Residual stress measurements

To determine residual stress distribution within CT specimens, X-ray diffraction measurements were carried out using Proto LXRD diffractometer (Proto Manufacturing Ltd.). An X-ray source with characteristic Mn K_α radiation (wavelength 2.10314 Å) was adopted for the measurement. Residual stresses were determined using the $\sin^2\psi$ method, collecting diffraction signal from {311} planes at Bragg angle 152.8° over beta angle range ±35°. Each measurement consisted of ten, 1s long exposures, while beta oscillation ±3° was employed. The measurements were performed at 5 different points on both sides of the CT specimen of B orientation, according to Fig. 1. The stresses in two orthogonal directions were determined for each point. Measurements were performed on CT specimens before cyclic loading. Center of examined area was approximately 5 mm in front of the notch tip. The area of measurement was chosen to be close to expected crack front position, once the threshold stress intensity factor will be reached. Prior to the measurement, a surface layer of 0.1 mm thickness was removed by electrolytic polishing to remove a layer of material affected by machining process.

2.3. Fatigue crack propagation measurements

The da/dN vs. ΔK curves were determined according to the standard ASTM E647 [29]. The tests were performed at room temperature, 50% relative humidity and load ratio $R = 0.1$, where R represents the ratio between minimal and maximal SIF during the loading cycle. The crack length was determined by optical measurements on both sides of specimen, which were mechanically polished prior to tests. Moreover, a COD gauge was used to determine the effective values of SIF. Tests were carried out using a universal testing machine with linear motor technology Instron E10000, at testing frequency of 70 Hz. Fatigue cracks were initiated from the manufactured notch applying higher loading than the expected SIF threshold. After crack propagation of at least 1 mm length, the procedure of load amplitude reduction was launched. The SIF was reduced by 5 % after crack increment approximately 0.1 mm, until no crack increment was recorded for at least 10^6 loading cycles. Afterwards, the corresponding SIF values were denoted as SIF threshold ΔK_{th}. The same procedure and experimental devices were used previously as described in more detail in Ref. [26].

Crack closure level was determined based on the compliance offset parameter defined in the ASTM E647 standard [29]. The standard assumes a 1%, 2% or 4% compliance offset for determination of crack closure. However, some authors question usability of these compliance offset limits. For example, Newman obtained better results when 0% compliance offset was used, which was determined from 1% to 2% compliance offsets, as presented in Ref. [30]. This indicates that actual crack closure is probably larger than value estimated according to the ASTM E647 standard. The SIF-compliance offset data measured for all investigated material states at a selected ΔK are presented in Fig. 2. The positive slope at higher loads is probably related to a different source of non-linearity than crack closure. Therefore, the crack closure level was determined as the point where the slope of the curve changes from negative to positive. Nevertheless, it is clear that crack closure for the AB and HT1 states was not present or is negligible. On the other hand, the specimen after HT2 exhibited quite high crack closure level.

2.4. Microstructure characterization

The microstructural changes resulting from the applied heat treatment were characterized using scanning (SEM) and transmission (TEM) electron microscopy. Samples for SEM were prepared by mechanical grinding followed by electrolytic polishing using a Struers LectroPol-5 polisher and solution of 600 ml methanol, 360 ml ethylene glycol monobuthyl ether and 60 ml perchloric acid. To conduct TEM observation, foils of approximately 80 μm thickness were mechanically prepared from AB, HT1 and HT2 samples and subsequently electrolytically polished using a Struers TenuPol-5 twin-jet polisher in solution of 95 % of acetic acid and 5 % of perchloric acid. Selected fatigue crack propagation tests were prematurely terminated to characterize microstructure in crack tip vicinity in the near-threshold SIF region – the tests were stopped after reaching the threshold SIF. Subsequently, FIB (Focused ion beam) lamellas for TEM investigation were prepared from the region in crack tip vicinity. To avoid microstructural observations close to free surface, CT specimens were longitudinally cut, and the lamellas were extracted from the specimen interior as schematically shown in Fig. 3. FIB lamellas were prepared by a Tescan Lyra3 dual beam field emission gun scanning electron microscope (SEM). The microstructure in the crack tip region was observed only for AB and HT2 specimens, since no significant microstructural changes were recorded in the case of HT1. The lamellas as well as the thin foils were examined by a Thermo Scientific Talos TEM operated at 200 kV. Moreover, transmission Kikuchi diffraction (TKD) and electron backscatter diffraction (EBSD) was employed using Oxford Symmetry S2 EBSD detector and AZtec software for post-acquisition analysis.

The microstructures of AB states and after both heat treatments are shown in Fig. 4. In case of the AB state, the microstructure contained

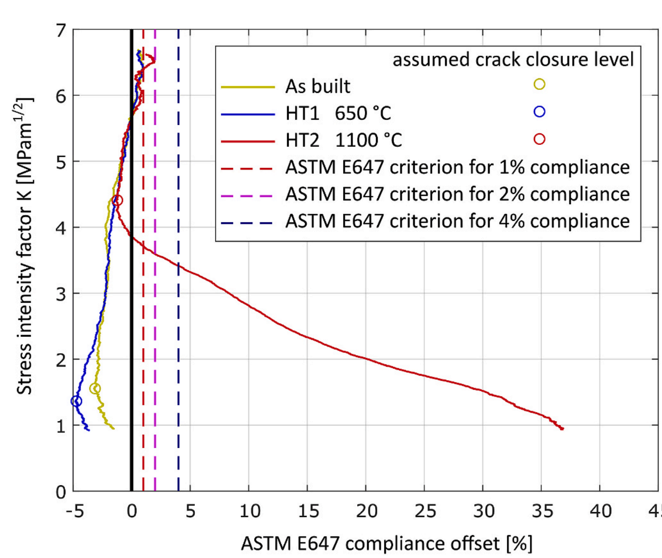

Fig. 2. The stress intensity factor – compliance offset plot for selected ΔK values. The crack closure was determined as the point where the slope of curve changes from negative to positive.

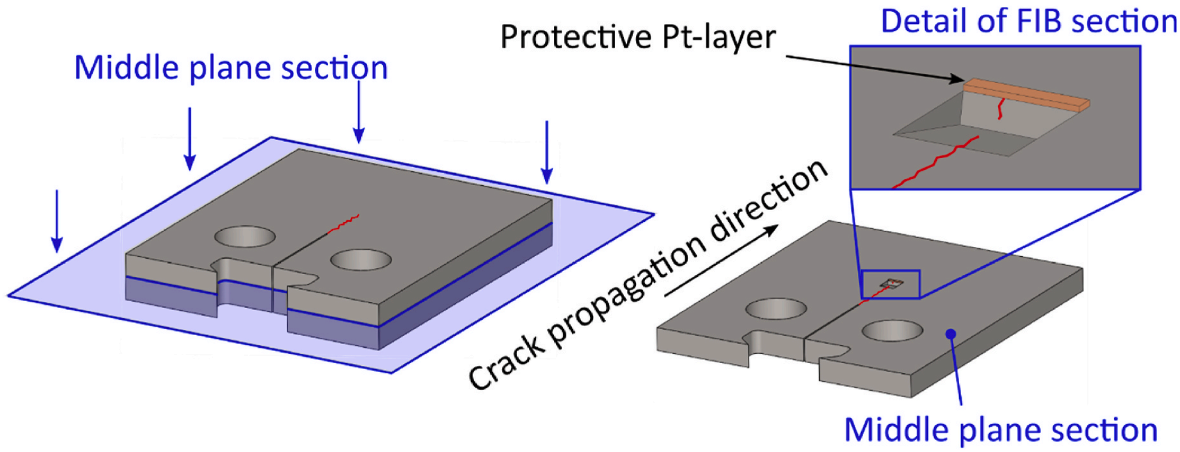

Fig. 3. Schematic description of FIB lamella extraction from fatigue crack tip of selected CT specimen.

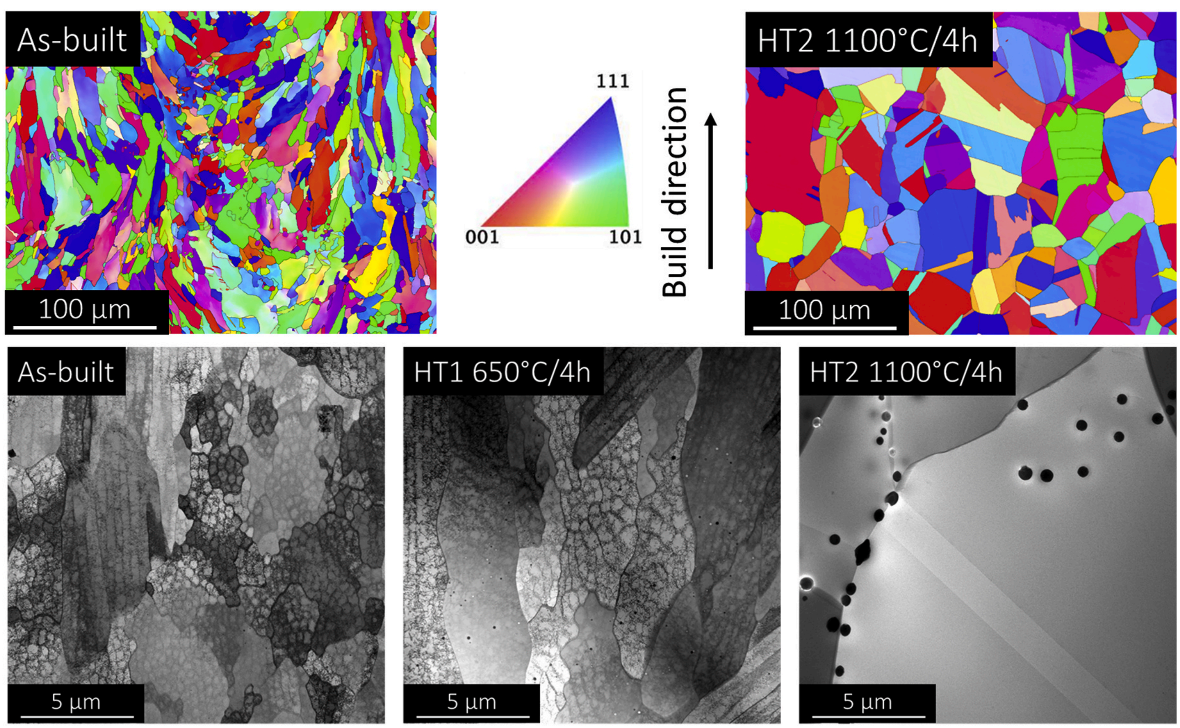

Fig. 4. Orientation EBSD maps and BF-STEM micrographs showing microstructure of as-built and heat-treated samples. As-built and HT1 exhibit fine grain microstructure with characteristic cell-substructure. After HT2 was observed nearly fully recrystallized microstructure, consisting of large polyhedral grains, almost free of dislocations and coarsened precipitates (dark particles).

characteristic cell-substructure with submicron size. Cell walls exhibited high dislocation density, while intracellular regions were almost dislocation-free. Cell walls were frequently decorated by amorphous oxide nanoprecipitates. The observed microstructure corresponds well with other investigations of L-PBF-processed austenitic stainless steels [3,4]. The application of HT1 did not significantly affect resulting microstructure. This was supported also by the hardness measurement, where the average hardness of 257.2 HV1 was identified for AB state and the average value of 253.3 HV1 was measured after HT1. Similarly to the AB state, microstructure after HT1 contained a submicron cell-substructure with high dislocation density within cell walls. The application of HT2 resulted in significant microstructural modifications. The microstructure was almost fully recrystallized (with more than 95% fraction of recrystallized grains) and consisted of coarse polyhedral austenitic grains with average size of 50 μm. The HT2 led to frequent nucleation of annealing twins and coarsening of oxide precipitates. Moreover, the cell-substructure completely diminished and recrystallized grains were almost dislocation-free. The microstructure after HT2 is comparable to wrought 304L steel which was reflected by significantly decreased average hardness of 164.1 HV1.

3. Results and discussion

3.1. Fatigue crack propagation in samples with different orientations

The results of fatigue crack propagation tests on the specimens with different orientations are shown in Fig. 5. The threshold SIF values (ΔK_{th}) were in the range of 2.7–3.1 MPa $m^{1/2}$, which is more likely a scatter in experimental data rather than a difference in behavior. Therefore, the results don't indicate any significant relation between the

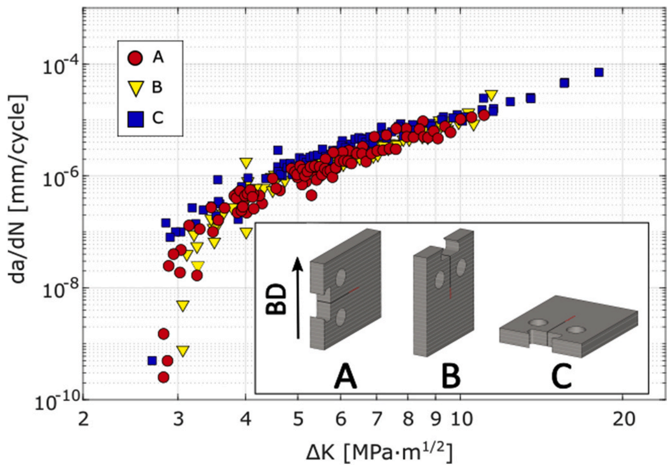

Fig. 5. Results of the fatigue crack propagation measurements for different orientations of specimens with respect to the build direction. The results indicate that the fatigue crack propagation behavior is independent of the specimen orientation.

fatigue crack behavior and the crack propagation direction with respect to the BD. The recorded threshold SIF range corresponds to the lowest values measured by Riemer et al. [21] and Fergani et al. [27]. However, they are significantly lower than the values recorded previously by Jambor et al. [26] for a wrought 304L stainless steel using the same specimen geometry and testing conditions (ΔK_{th} was above 5 MPa m$^{1/2}$). The absence of specimen orientation effect contradicts the findings in Refs. [21,22]. Generally, one of the possible explanations is the presence of residual stresses with different magnitudes along various orientations. Although there was reported no effect of build-in residual stresses on the fatigue crack propagation in L-PBF-processed austenitic stainless steels [21], Fergani et al. [27] showed that quenched-in compressive residual stresses can enhance crack propagation resistance. Therefore, the residual stress measurements were performed in order to reveal the actual residual stress state in studied CT specimens. The results shown in Fig. 6, indicate high values of tensile residual stresses in both measured directions. The character of residual stresses is similar to the results of Riemer et al. [21] postulating no significant effect on the fatigue crack propagation. Therefore, the recorded residual stresses cannot explain the absence of orientation effect. Possible explanation can be found in the significantly higher yield strength of material presented in this study, 592 MPa, compared with 462 MPa of L-PBF 316L stainless steel examined in Ref. [21]. The high value of yield strength results in very limited size of crack tip plastic zone in comparison with the average grain size. The well-known effective hindering of dislocation motion by the dislocation cell-substructure [3] presumably overshadowed the back-stresses related with grain boundaries. Therefore, the structure variability inherited from L-PBF process seems to have limited effect on fatigue crack propagation.

3.2. Effect of heat treatment on fatigue crack propagation

Investigation of heat treatment effect on the fatigue crack propagation was carried out using A type of CT specimens (see Fig. 1). The aim was to assess the possible effect of characteristic as-built microstructure on the low ΔK_{th} values, recorded for L-PBF materials in this study and also by other authors [21,27]. The results of the fatigue crack propagation tests performed on AB and heat-treated specimens are shown in Fig. 7. Determined threshold stress intensity factor for AB ($\Delta K_{th} \approx 2.7$ MPa m$^{1/2}$) is low and is close to the theoretical values, when the crack closure is completely absent [31]. The measurement of the effective stress intensity factors using COD gauge supports these findings. The plot in Fig. 8 shows a dependence of the U parameter (ratio between effective and applied SIF) on applied ΔK. The values close to 0.9 and 1 indicate that the crack was opened within the whole loading cycle. Similar results were obtained also for the specimens after HT1. Such behavior is totally different, compared to wrought AISI 304L steel, where crack closure was always present at low stress asymmetry ratios [26]. Microstructures of AB and HT1 states are nearly identical, however, the heat-treated specimens are relieved from macroscopic residual stresses. Therefore, it can be claimed, that the residual stresses aren't the cause of the observed anomalous behavior. This corresponds well with

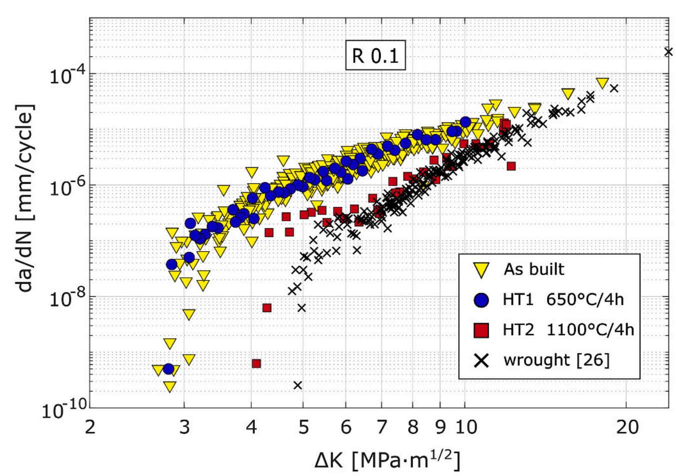

Fig. 7. Plot of *da/dN-ΔK* curves representing effect of heat treatment on the fatigue crack propagation behavior. The results obtained on wrought 304L [26] were included for direct comparison with conventionally-processed material. The threshold stress intensity factors ΔK_{th} for AB and HT1 specimen series are significantly lower than the values measured for HT2 specimen series and conventional–wrought material.

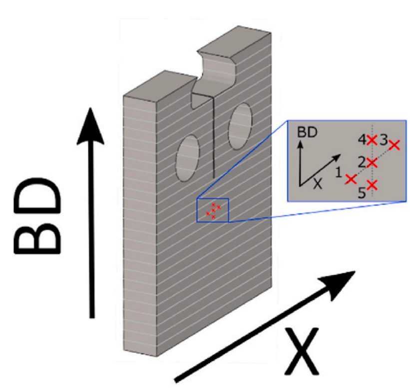

Point	BD direction	X direction
1	461	455
2	366	446
3	340	316
4	494	555
5	386	403

residual stress value [MPa]

Fig. 6. Schematic picture showing position and orientation of measured residual stresses. Distance between point was approximately 1 mm in both directions.

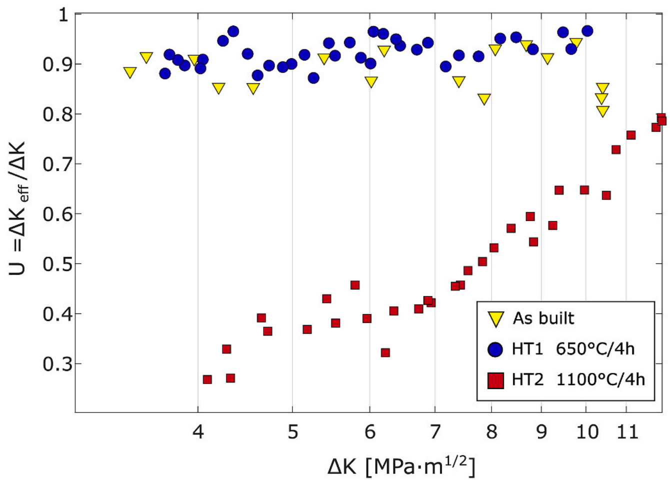

Fig. 8. The dependence of U parameter on ΔK. While for AB and HT1 series the crack closure is absent, its presence can be easily recognized after applying HT2.

the findings of other authors [21,27], who reported that relieving of the built-in residual stresses did not affect the resulting crack propagation behavior.

A significant change in the fatigue crack propagation behavior was recorded for the HT2 specimens. In this case, the determined fatigue crack propagation behavior better corresponds with that of wrought 304L steel, with the threshold SIF ΔK_{th} higher than 4 MPa m$^{1/2}$. The difference (≈1.3 MPa m$^{1/2}$) between the threshold SIFs in AB (2.7 MPa m$^{1/2}$) and HT2 state (4 MPa m$^{1/2}$) means a relative increase by 48 %. Such significant difference can have a significant impact on residual lifetime of structural components [28]. An increase in the threshold SIF after high-temperature annealing (1050 °C/1 h) was also reported by Fergani et al. [27], however less significant (from 2.9 MPa m$^{1/2}$ to 3.4 MPa m$^{1/2}$). This can be attributed to the parameters of applied heat treatment, which resulted just in partially recrystallized microstructure, whereas the microstructure after HT2 was nearly fully recrystallized. The measurement of COD near the crack propagation threshold for HT2 specimen series showed (Fig. 8) a considerable level of crack closure, which is typical for conventional materials at low load ratio in the near-threshold region. The similar behavior of L-PBF-processed alloy after HT2 and wrought 304L counterpart demonstrate that the characteristic cell-substructure is responsible for the observed anomalous fatigue crack propagation behavior. The absence of crack closure (both - oxide and plasticity-induced) leading to lower threshold SIF for L-PBF-processed stainless steels was proposed as a plausible explanation also by Suryawanshi et al. [22], however, without providing further details.

Since the different fatigue crack propagation behavior was attributed to the presence/absence of crack closure phenomenon, individual mechanisms of crack closure [32–34] and their contributions are addressed in the further text.

Roughness-induced crack closure – Microscopically rough fracture surfaces can cause their premature contact, due to the mutual misfit [35]. The L-PBF nature of the AB microstructure can be considered fine-grained, and thus the fracture surface roughness is considerably small. The application of HT1 does not modify the grain structure, therefore no change in the fracture surface morphology can be expected. The microstructure modification after HT2 is more severe, reflected by more than 95% fraction of recrystallized microstructure, resulting in polyhedral austenitic grains of average size 50 μm. Such coarse microstructure can produce much more torturous crack path than the fine L-PBF microstructure due to significantly larger dislocation free path, as documented by Fig. 9. In combination with a greater asymmetry of slip with respect to the crack plane, the effect of roughness-induced crack closure on the effective SIF range can be expected to be much larger for the HT2 series. Therefore, the character of microstructure and the related roughness-induced crack closure are assumed to contribute significantly to the observed differences in crack growth behavior. A similar effect on fatigue crack growth rate and threshold values was observed by Leitner et al. [36], where the ultra-fine-grained microstructure resulted in a complete elimination of crack closure. The results from AB and HT1 specimens indicate that the submicron cell-substructure could may have the same effect.

Plasticity-induced crack closure – It is generally accepted that irreversible plastic flow in the crack tip vicinity is the cause of plasticity-induced crack closure [32,33,35,37]. Fig. 8 shows increasing significance of crack closure for smaller loading amplitudes. However, even under large amplitudes in the Paris regime, crack closure is smaller in AB and HT1 microstructures than in HT2, which means that the plasticity-induced crack closure component was also different. In order to better understand differences between crack tip zone cyclic deformation, the microstructure of the crack tip area of AB and HT2 series are shown in Fig. 10. In the case of AB state, the crack tip is enveloped by deformation-induced α′-martensite. The cell-substructure in austenite matrix is well-preserved even in the crack tip vicinity, and there are no signs of significant dislocation activity at larger distances from crack tip. Most of the plastic deformation is accommodated by transformed α′-martensite and surrounding austenite matrix in close vicinity of the fatigue crack. This suggest limited monotonic plastic zone size and relatively large portion of reversible plastic flow due to high dislocation back-stress. After dissolution of initial cell-substructure by applying HT2, intensive dislocation activity with planar character can be seen in the crack tip vicinity, suggesting significantly larger size of plastic zone compared to as-built state.

L-PBF process produces a specific microstructure with hardness higher by almost 60 % than recrystallized state (257 HV1 vs. 164 HV1). In AB condition, material is similar to intensively cold-worked austenitic stainless steel, which usually exhibited cyclic softening independent of the applied strain amplitude [38]. Considering the results published in Ref. [39], where it is stated that strain-induced martensite has only 25 % higher hardness than conventionally processed austenitic matrix, it can be assumed that L-PBF produced austenitic structure in its AB state is

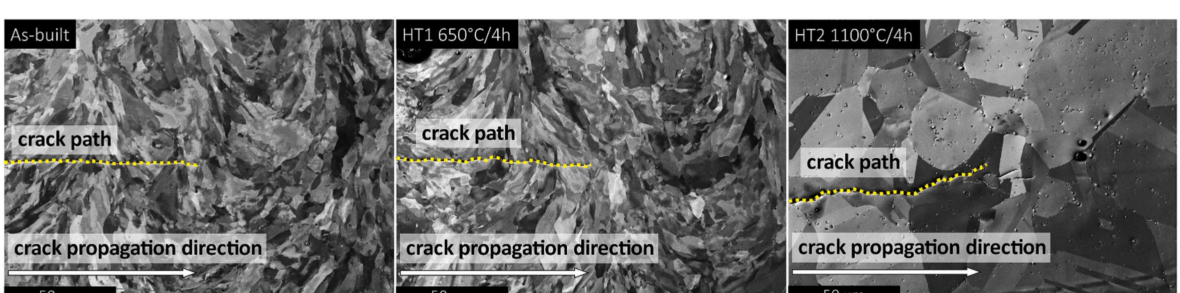

Fig. 9. Comparison of the crack profiles in the near-threshold region (SEM). Higher crack tortuosity in the case of HT2 is clearly visible.

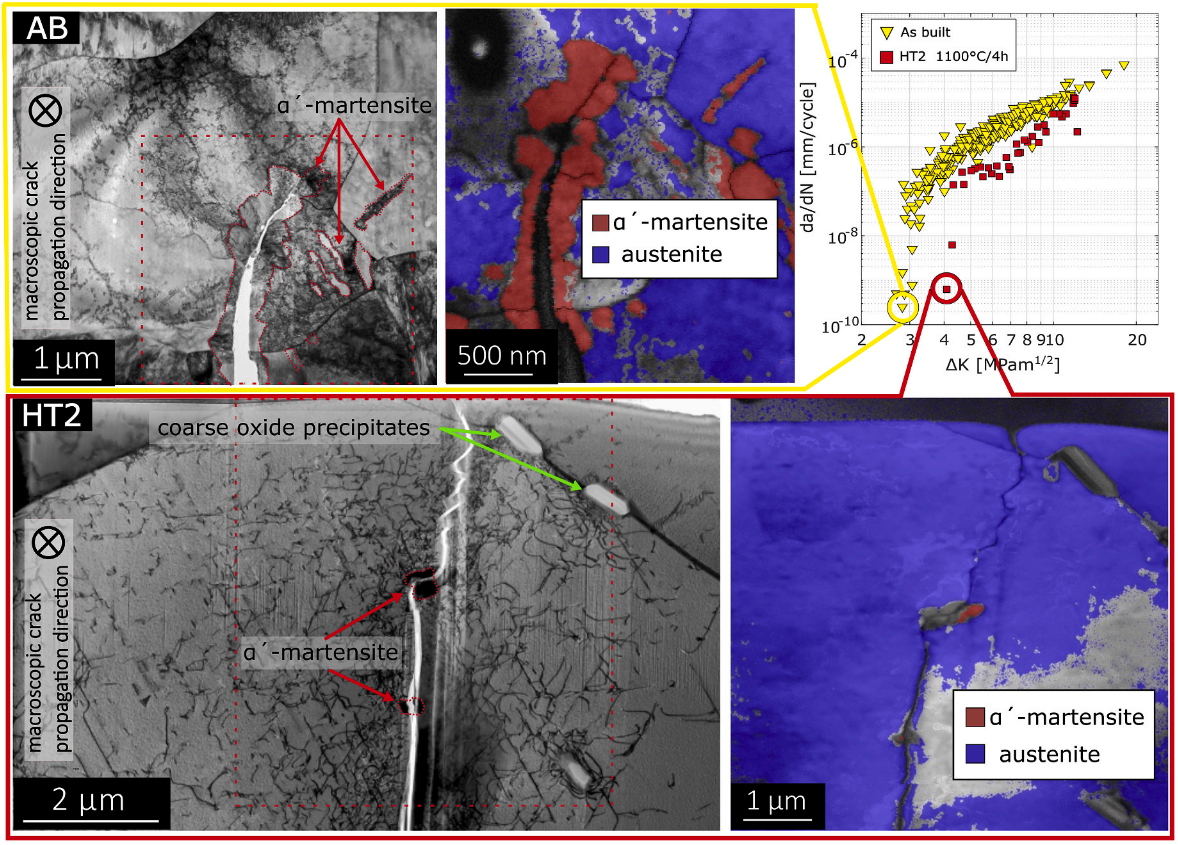

Fig. 10. Microstructure of the crack tip area in the fatigue crack propagation threshold region observed by TEM (STEM-BF) with corresponding phase maps acquired by TKD. Orientation of the extracted lamellas is schematically shown in Fig.3. The differences in plastic deformation behavior in the crack tip vicinity are clearly depicted. In AB state, a thin layer of α′-martensite is formed along the crack zone, while the dislocation cell-substructure is preserved even in close vicinity to the fatigue crack. This suggests that the cyclic plastic deformation is limited to a small region of austenitic matrix and deformation-induced α′-martensite in close proximity to the fatigue crack. After HT2, the microstructure is similar to the conventionally processed stainless steels and the extensive slip with planar character is visible.

much harder than strain-induced martensite. Therefore, ongoing martensitic transformation in the crack tip vicinity causes local cyclic softening and, thus, the plastic deformation was localized within a transformed areas and adjacent softened austenitic matrix regions close to the crack tip. In such a condition, irreversible plastic flow was significantly reduced and, thus, the contribution of plasticity-induced crack closure diminished [37]. The traditional models consider only monotonic plasticity behavior of materials into account and in most of them the parameter U is predicted as about 0.8 for plane strain at $R = 0.1$ [40,41]. However, cyclic softening is expected to significantly reduce plasticity-induced crack closure [36]. Authors believe that the presence of a thin martensite layer is not a necessity, and the same behavior would have been recorded even without it, due to the cyclic softening nature of the AB microstructure of L-PBF-processed austenitic stainless steel evidenced by multiple fatigue studies [42,43].

Since the application of HT1 didn't result in any significant microstructural changes, the deformation behavior modifications cannot be expected near the crack tip. After HT2, nearly full recrystallization of microstructure occurred and, therefore the microstructure is comparable with the wrought austenitic stainless steels. Annealed austenitic microstructure exhibits extensive cyclic hardening [44,45], where the size of forward cyclic plastic zone is significantly larger than the reverse one, implicating large irreversible plastic flow and vigorous contribution of the plasticity-induced crack closure on the resulting crack propagation behavior.

Oxide-induced crack closure – This closure mechanism can significantly affect crack propagation rates, especially in the region close to the threshold SIFs [46–48]. Although applied heat treatment reduces chemical segregation of Cr and Mn formed due to the L-PBF process, it has a little effect on the overall oxide formation. Therefore, no substantial differences in oxide formation can be expected for the examined states due to changes in chemical segregation. On the other hand, differences in plasticity- and roughness-induced crack closures could affect oxide debris formation [46]. The oxide debris layer is produced by fretting, for which repetitive rubbing of fracture surfaces under large compressive stress is needed. The contact pressure is expected to be influenced by plasticity-induced crack closure and the amount of friction depends on shear displacement resulting from roughness and mismatch of the mating surfaces. Therefore, this component is assumed to be reduced in the case of the fine-grain microstructure in AB and HT1 series.

Trying to generalize these findings, the explanation of low threshold SIF provided in the present study can be applied also to the results of other authors. Riemer et al. [21] as well as Fergani et al. [27] reported very low threshold SIF values for L-PBF austenitic stainless steels. In their studies, there wasn't recorded presence of α′-martensite layer in the crack tip vicinity. This confirms the assumption, that the characteristic dislocation cell-substructure formed during L-PBF process and its properties is most likely the cause for the unusually low threshold SIF in L-PBF austenitic stainless steels, due significant reduction of crack closure mechanism. Phase transformation of austenite into α′-martensite is accompanied by approximately 2 % volume increase [49] which causes compressive residual stresses enhancing crack closure effects and is one of the mechanisms how TRIP (TRansformation Induced Plasticity) phenomenon improves crack propagation resistance [49]. Despite that fact, no crack closure was observed in the case of AB series in the present study. Authors attributed this to the small thickness of deformation induced α′-martensite layer, ranging from 100 nm up to 500 nm (Fig. 10), where total net contribution of the volume change can be neglected. Kumar et al. [25] reported a presence of not negligible crack closure in L-PBF 304L steel and explained it by the presence of stress-induced α′-martensite. In their study, the thickness of martensite layer in the threshold region was about 10 μm, which is almost by two orders of magnitudes larger than in the case of the present investigation. This can be attributed to significantly higher austenite metastability, which exhibited a certain volume fraction of martensite already in undeformed microstructure. Therefore, austenitic stainless steels produced by L-PBF exhibits very low threshold SIF due to the absence of crack closure mechanisms stemming from the specific microstructure inherited by rapid solidification, unless extremely high susceptibility to the TRIP effect is present.

4. Conclusions

Based on the performed experiments and thorough data analysis, the following conclusions can be drawn.

- Austenitic stainless steel 304L prepared by L-PBF process exhibited significantly lower resistance to fatigue crack propagation compared with its wrought counterparts.
- The low resistance to the fatigue crack propagation at low stress ratios ($R = 0.1$), especially in the near-threshold region, was explained by the absence of crack closure effect.
- Application of heat treatments revealed that the absence of crack closure was not caused by the presence of residual stress fields, but by the specific nature dislocation cell-substructure. It is assumed that this structure resulted in elimination of both plasticity- and roughness-induced crack closure.
- The as-built microstructure containing sub-micron dislocation cell-substructure is prone to cyclic instability. In the crack tip region, cyclic plasticity results in strain-induced phase transformation and continuous thin martensitic layer is formed. The deformation-induced martensite phase is softer compared to the austenite matrix strengthened by the cell-substructure which together with cyclic instability of the matrix resulted in local cyclic softening of the crack tip region. In such conditions, the formation of the plasticity-induced and roughness-induced crack closure were significantly reduced, leading to a low macroscopic resistance to the fatigue crack propagation.

CRediT authorship contribution statement

Michal Jambor: Writing – original draft, Investigation, Conceptualization. **Tomáš Vojtek:** Data curation, Writing – review & editing. **Pavel Pokorný:** Data curation, Investigation, Writing – review & editing. **Daniel Koutný:** Investigation, Writing – review & editing. **Luboš Náhlík:** Project administration, Funding acquisition, Supervision. **Pavel Hutař:** Project administration, Funding acquisition, Supervision. **Miroslav Šmíd:** Project administration, Funding acquisition, Supervision, Writing – review & editing.

Declaration of competing interest

The authors declare that they have no known competing financial interests or personal relationships that could have appeared to influence the work reported in this paper.

Data availability

Data will be made available on request.

Acknowledgements

The authors are grateful for the financial support of the Czech Science Foundation by the projects 19-25571Y and 22-28283S. The authors would like to thank also for the support from European Union's Horizon 2020 research and innovation program (H2020-WIDESPREAD-2018, SIRAMM) under grant agreement No 857124.

References

[1] F. Brenne, T. Niendorf, H.J. Maier, Additively manufactured cellular structures: impact of microstructure and local strains on the monotonic and cyclic behavior under uniaxial and bending load, J. Mater. Process. Technol. 213 (9) (2013) 1558–1564.
[2] E. MacDonald, R. Wicker, Multiprocess 3D printing for increasing component functionality, Science 353 (6307) (2016), aaf2093.
[3] L. Liu, Q. Ding, Y. Zhong, J. Zou, J. Wu, Y.-L. Chiu, J. Li, Z. Zhang, Q. Yu, Z. Shen, Dislocation network in additive manufactured steel breaks strength–ductility trade-off, Mater. Today 21 (4) (2018) 354–361.
[4] J.G. Kim, J.B. Seol, J.M. Park, H. Sung, S.H. Park, H.S. Kim, Effects of cell network structure on the strength of additively manufactured stainless steels, Met. Mater. Int. 27 (8) (2021) 2614–2622.
[5] H. Zhang, M. Xu, P. Kumar, C. Li, W. Dai, Z. Liu, Z. Li, Y. Zhang, Enhancement of fatigue resistance of additively manufactured 304L SS by unique heterogeneous microstructure, Virtual Phys. Prototyp. 16 (2) (2021) 125–145.
[6] J.P. Kruth, P. Mercelis, J. Van Vaerenbergh, L. Froyen, M. Rombouts, Binding mechanisms in selective laser sintering and selective laser melting, Rapid Prototyp. J. 11 (1) (2005) 26–36.
[7] C. Qiu, M.A. Kindi, A.S. Aladawi, I.A. Hatmi, A comprehensive study on microstructure and tensile behaviour of a selectively laser melted stainless steel, Sci. Rep. 8 (1) (2018) 7785.
[8] M. Tang, P.C. Pistorius, S. Narra, J.L. Beuth, Rapid solidification: selective laser melting of AlSi10Mg, J. Occup. Med. 68 (3) (2016) 960–966.
[9] D. Kong, C. Dong, X. Ni, L. Zhang, X. Li, Cellular size dependence on the strength of additively manufactured austenitic stainless steel, Mater. Lett. 279 (2020), 128524.
[10] Z. Li, B. He, Q. Guo, Strengthening and hardening mechanisms of additively manufactured stainless steels: the role of cell sizes, Scripta Mater. 177 (2020) 17–21.
[11] O.O. Salman, C. Gammer, A.K. Chaubey, J. Eckert, S. Scudino, Effect of heat treatment on microstructure and mechanical properties of 316L steel synthesized by selective laser melting, Mater. Sci. Eng. 748 (2019) 205–212.
[12] N. Chen, G. Ma, W. Zhu, A. Godfrey, Z. Shen, G. Wu, X. Huang, Enhancement of an additive-manufactured austenitic stainless steel by post-manufacture heat-treatment, Mater. Sci. Eng. 759 (2019) 65–69.
[13] H. Yin, M. Song, P. Deng, L. Li, B.C. Prorok, X. Lou, Thermal stability and microstructural evolution of additively manufactured 316L stainless steel by laser powder bed fusion at 500–800°C, Addit. Manuf. 41 (2021), 101981.
[14] B. Blinn, M. Klein, C. Gläßner, M. Smaga, J.C. Aurich, T. Beck, An investigation of the microstructure and fatigue behavior of additively manufactured AISI 316L stainless steel with regard to the influence of heat treatment, Metals (2018).
[15] C. Elangeswaran, A. Cutolo, G.K. Muralidharan, C. de Formanoir, F. Berto, K. Vanmeensel, B. Van Hooreweder, Effect of post-treatments on the fatigue behaviour of 316L stainless steel manufactured by laser powder bed fusion, Int. J. Fatig. 123 (2019) 31–39.
[16] W.-S. Shin, B. Son, W. Song, H. Sohn, H. Jang, Y.-J. Kim, C. Park, Heat treatment effect on the microstructure, mechanical properties, and wear behaviors of stainless steel 316L prepared via selective laser melting, Mater. Sci. Eng. 806 (2021), 140805.
[17] S. Dryepondt, P. Nandwana, P. Fernandez-Zelaia, F. List, Microstructure and high temperature tensile properties of 316L fabricated by laser powder-bed fusion, Addit. Manuf. 37 (2021), 101723.
[18] D. Kong, X. Ni, C. Dong, L. Zhang, C. Man, J. Yao, K. Xiao, X. Li, Heat treatment effect on the microstructure and corrosion behavior of 316L stainless steel fabricated by selective laser melting for proton exchange membrane fuel cells, Electrochim. Acta 276 (2018) 293–303.
[19] Q. Chao, V. Cruz, S. Thomas, N. Birbilis, P. Collins, A. Taylor, P.D. Hodgson, D. Fabijanic, On the enhanced corrosion resistance of a selective laser melted austenitic stainless steel, Scripta Mater. 141 (2017) 94–98.
[20] M.M. Mirsayar, A generalized criterion for fatigue crack growth in additively manufactured materials – build orientation and geometry effects, Int. J. Fatig. 145 (2021), 106099.
[21] A. Riemer, S. Leuders, M. Thöne, H.A. Richard, T. Tröster, T. Niendorf, On the fatigue crack growth behavior in 316L stainless steel manufactured by selective laser melting, Eng. Fract. Mech. 120 (2014) 15–25.
[22] J. Suryawanshi, K.G. Prashanth, U. Ramamurty, Mechanical behavior of selective laser melted 316L stainless steel, Mater. Sci. Eng. 696 (2017) 113–121.
[23] H. Zhu, Q. Pan, K. Zhang, C. Zhou, W. Zhang, Y. Yao, D. Ying, Y. He, J. Zheng, L. Zhang, The difference in fatigue crack growth induced by internal and external hydrogen in selective laser melted 304L stainless steel, Int. J. Fatig. 163 (2022), 107052.
[24] A. Riemer, H.A. Richard, Crack propagation in additive manufactured materials and structures, Procedia Struct. Integr. 2 (2016) 1229–1236.

[25] P. Kumar, R. Jayaraj, Z. Zhu, R.L. Narayan, U. Ramamurty, Role of metastable austenite in the fatigue resistance of 304L stainless steel produced by laser-based powder bed fusion, Mater. Sci. Eng. 837 (2022), 142744.

[26] M. Jambor, T. Vojtek, P. Pokorný, M. Šmíd, Effect of solution annealing on fatigue crack propagation in the AISI 304L TRIP steel, Materials (2021).

[27] O. Fergani, A. Bratli Wold, F. Berto, V. Brotan, M. Bambach, Study of the effect of heat treatment on fatigue crack growth behaviour of 316L stainless steel produced by selective laser melting, Fatig. Fract. Eng. Mater. Struct. 41 (5) (2018) 1102–1119.

[28] P. Pokorný, P. Hutař, L. Náhlík, Residual fatigue lifetime estimation of railway axles for various loading spectra, Theor. Appl. Fract. Mech. 82 (2016) 25–32.

[29] E. Astm, Standard test method for measurement of fatigue crack growth rates, Annu. Book ASTM Stand. 3 (2011) 591–630, 647.

[30] J.C. Newman, K.F. Walker, Fatigue-crack growth in two aluminum alloys and crack-closure analyses under constant-amplitude and spectrum loading, Theor. Appl. Fract. Mech. 100 (2019) 307–318.

[31] B. Li, L.G. Rosa, Prediction models of intrinsic fatigue threshold in metal alloys examined by experimental data, Int. J. Fatig. 82 (2016) 616–623.

[32] A.J. McEvily, K. Minakawa, On crack closure and the notch size effect in fatigue, Eng. Fract. Mech. 28 (5) (1987) 519–527.

[33] P. Pokorný, T. Vojtek, L. Náhlík, P. Hutař, Crack closure in near-threshold fatigue crack propagation in railway axle steel EA4T, Eng. Fract. Mech. 185 (2017) 2–19.

[34] R. Pippan, G. Strobl, H. Kreuzer, C. Motz, Asymmetric crack wake plasticity – a reason for roughness induced crack closure, Acta Mater. 52 (15) (2004) 4493–4502.

[35] R. Pippan, A. Hohenwarter, Fatigue crack closure: a review of the physical phenomena, Fatig. Fract. Eng. Mater. Struct. 40 (4) (2017) 471–495.

[36] T. Leitner, A. Hohenwarter, R. Pippan, Revisiting fatigue crack growth in various grain size regimes of Ni, Mater. Sci. Eng. 646 (2015) 294–305.

[37] D.M. Rodrigues, F.V. Antunes, Finite element simulation of plasticity induced crack closure with different material constitutive models, Eng. Fract. Mech. 76 (9) (2009) 1215–1230.

[38] V.S. Srinivasan, R. Sandhya, M. Valsan, K. Bhanu Sankara Rao, S.L. Mannan, Comparative evaluation of strain controlled low cycle fatigue behaviour of solution annealed and prior cold worked 316L(N) stainless steel, Int. J. Fatig. 26 (12) (2004) 1295–1302.

[39] A. Weidner, U.D. Hangen, H. Biermann, Nanoindentation measurements on deformation-induced α'-martensite in a metastable austenitic high-alloy CrMnNi steel, Phil. Mag. Lett. 94 (8) (2014) 522–530.

[40] J.C. Newman, A crack opening stress equation for fatigue crack growth, Int. J. Fract. 24 (4) (1984) R131–R135.

[41] J.J.A. van Kuijk, R.C. Alderliesten, R. Benedictus, Unraveling the myth of closure corrections: sharpening the definition of opening and closure stresses with an energy approach, Int. J. Fatig. 143 (2021), 106016.

[42] C.-H. Yu, A. Leicht, R.L. Peng, J. Moverare, Low cycle fatigue of additively manufactured thin-walled stainless steel 316L, Mater. Sci. Eng. 821 (2021), 141598.

[43] Y. Chen, X. Wang, J. shen, Y. Peng, Y. Jiang, X. Yang, S.B. Leen, J. Gong, Deformation mechanisms of selective laser melted 316L austenitic stainless steel in high temperature low cycle fatigue, Mater. Sci. Eng. 843 (2022), 143123.

[44] M. Šmíd, I. Kuběna, M. Jambor, S. Fintová, Effect of solution annealing on low cycle fatigue of 304L stainless steel, Mater. Sci. Eng. 824 (2021), 141807.

[45] D. Ye, S. Matsuoka, N. Nagashima, N. Suzuki, The low-cycle fatigue, deformation and final fracture behaviour of an austenitic stainless steel, Mater. Sci. Eng. 415 (1) (2006) 104–117.

[46] M. Madia, T. Vojtek, L. Duarte, U. Zerbst, P. Pokorný, M. Jambor, P. Hutař, Determination of fatigue crack propagation thresholds for steel in presence of environmental effects, Int. J. Fatig. 153 (2021), 106449.

[47] P. Pokorný, T. Vojtek, M. Jambor, L. Náhlík, P. Hutař, Effect of underload cycles on oxide-induced crack closure development in Cr-Mo low-alloy steel, Materials (2021).

[48] T. Vojtek, P. Pokorný, I. Kuběna, L. Náhlík, R. Fajkoš, P. Hutař, Quantitative dependence of oxide-induced crack closure on air humidity for railway axle steel, Int. J. Fatig. 123 (2019) 213–224.

[49] Z. Mei, J.W. Morris, Influence of deformation-induced martensite on fatigue crack propagation in 304-type steels, Metall. Trans. A 21 (12) (1990) 3137–3152.